九州工業大学学術機関リポジトリ
Kyutacar
Kyushu Institute of Technology Academic Repository

Measurement of Excited States of Sb Impurity in Si by Traveling-Wave Method

著者	Sun Yong, Takase Tsuyoshi, Sakaino Masamichi, Miyasato Tatsuro
journal or publication title	Journal of Applied Physics
volume	112
number	013709
page range	1-8
year	2012-07-06
URL	http://hdl.handle.net/10228/5857

doi: info:doi/10.1063/1.4731736

AIP | Journal of Applied Physics

Measurement of excited states of Sb impurity in Si by traveling–wave method

Yong Sun, Tsuyoshi Takase, Masamichi Sakaino, and Tatsuro Miyasato

Citation: Journal of Applied Physics **112**, 013709 (2012); doi: 10.1063/1.4731736
View online: http://dx.doi.org/10.1063/1.4731736
View Table of Contents: http://scitation.aip.org/content/aip/journal/jap/112/1?ver=pdfcov
Published by the AIP Publishing

Articles you may be interested in

Donor behavior of Sb in ZnO
J. Appl. Phys. **112**, 033706 (2012); 10.1063/1.4742984

Hot hole redistribution in impurity states of boron-doped silicon terahertz emitters
J. Appl. Phys. **98**, 093710 (2005); 10.1063/1.2128045

Terahertz optically pumped Si:Sb laser
J. Appl. Phys. **92**, 5632 (2002); 10.1063/1.1515377

Characterization by medium energy ion scattering of damage and dopant profiles produced by ultrashallow B and As implants into Si at different temperatures
J. Vac. Sci. Technol. B **20**, 974 (2002); 10.1116/1.1477420

Counterdoped very shallow p + /n junctions obtained by B and Sb implantation and codiffusion in Si
J. Appl. Phys. **83**, 1742 (1998); 10.1063/1.366893

AIP | Journal of Applied Physics
INTRODUCING INVITED PERSPECTIVES
Ultrafast magnetism and THz spintronics
Authors: Jakob Walowski and Markus Münzenberg

Reuse of AIP Publishing content is subject to the terms at: https://publishing.aip.org/authors/rights-and-permissions. Download to IP: 150.69.123.200 On: Wed, 26 Oct 2016 05:48:03

Measurement of excited states of Sb impurity in Si by traveling–wave method

Yong Sun, Tsuyoshi Takase,[a] Masamichi Sakaino,[b] and Tatsuro Miyasato
Department of Applied Science for Integrated System Engineering, Kyushu Institute of Technology, 1-1 Sensui-machi, Tobata, Kitakyushu, Fukuoka 804-8550, Japan

(Received 9 January 2012; accepted 30 May 2012; published online 6 July 2012)

The ground and excited states of Sb atom in Si, 1*s* (A_1), 1*s* (T_2), 1*s* (*E*), and $2p^0$, were measured by using a traveling-wave method. The Sb-doped Si crystal with donor concentration of $2 \times 10^{15}\,cm^{-3}$ was placed the distance of 5 μm above a piezoelectric crystal in the fringe field of a surface acoustic wave. The free electrons excited from the bound states of the Sb atom are drifted by the traveling-wave, and thus lose their energy as the Joule heat through lattice and ion scattering processes. A strong temperature-dependent energy loss of the traveling-wave can be observed at temperatures below 200 K. The values of the bound states of the Sb atom can be characterized by using the Arrhenius plot for thermal activation process of the electrons in the bound states. The measurements were carried out at two frequencies of the traveling-wave, 50 MHz and 200 MHz. At the frequency of 50 MHz, the dielectric properties of the Si crystal are governed by dopant polarization but by electronic polarization at 200 MHz. We found that measurement accuracy of the bound states depends mainly on the electron mobility and the dielectric constant of the Si crystal, which are sensitive to the frequency and strength of the traveling-wave as well as electronic polarization properties of the Si crystal. © *2012 American Institute of Physics*. [http://dx.doi.org/10.1063/1.4731736]

I. INTRODUCTION

The bound states of an impurity atom doped in semiconductor have been an important parameter for electronic applications, such as far-infrared active laser medium based on neutral donor intracenter optical transitions[1,2] and quantum computer using impurity nuclei as qubits.[3,4] For an example of Sb–doped Si, the bound states of Sb atom, 1*s* (A_1), 1*s* (T_2), 1*s* (*E*), and $2p^0$ are 42.7 meV, 32.9 meV, 30.6 meV, and 11.5 meV below the conduction band edge with spacings of 9.8 meV, 2.3 meV, and 19.1 meV.[5] In general, the bound states are obtained by far-infrared absorption measurement.[6,7] Several electrical measurement techniques have been used to estimate the ionization energy of impurity atoms in semiconductors through Arrhenius plot using a temperature-dependent carrier concentration. In the case of Sb–doped Si, the ionization of Sb atom is observed in the temperature range of $20 \sim 60$ K, corresponding to the energy k_BT from 1.7 to 5.2 meV where k_B is Boltzmann constant and T is absolute temperature. Therefore, the Arrhenius plot cannot estimate each bound states of the Sb atom and only observed lowest one from among many bound states as ionization energy due to the k_BT close to the spacings of the states.

Thermal admittance spectroscopy is a powerful tool to investigate ionization energy and capture cross section about impurity atoms[8] and to determine band offsets in various semiconductor material systems.[9] This technique is based on a strong dependence of the semiconductor junction differential admittance on both temperature and measurement ac signal frequency. The real part of the junction admittance, the conductance, exhibits a peak on its temperature dependence when the impurity ionization time constant is comparable with the ac measurement signal period.[10] It measures the carriers undergoing a dynamic emission and capture process among the impurities.

The Hall-effect measurements enable us to determine the ionization energy for doped semiconductors through fitting the curves of the ionized carrier concentration against inverse absolute temperature.[11] It measures the free carriers from the Hall voltage under dc bias and applied magnetic field under thermal equilibrium.

The bound states of a doped impurity atom in semiconductor have been studied theoretically and experimentally, but they cannot be obtained by measuring temperature-dependent conductivity, admittance, and Hall constant of the semiconductor. In this study, we extended a traveling-wave method to determine the bound states of the Sb atom in Si crystal for the first time. In this method, we measure the Joule loss of the free carriers drifted by the traveling-wave. A strong temperature dependence of the loss enables us to obtain four bound states of the Sb atom in Si from 1*s* (A_1) to $2p^0$.

A surface acoustic wave (SAW) interacts with the electrons of a semiconductor when the semiconductor is placed near the surface of the piezoelectric crystal. This acoustoelectric (AE) effect for a SAW traveling in the semiconductor gives rise to a longitudinal d.c. acoustoelectric voltage. The theory and measurement of the d.c acoustoelectric voltage or current are well known.[12–16]

The traveling-wave method for measuring drift mobilities of semiconductors was introduced thirty years ago.[17]

[a]Present address: The School of International Languages and Cultures, Baiko Gakuin University, Koyocho 1-1-1, Shimonoseki, Yamaguchi 750-8511, Japan.
[b]Present address: Department of Vehicle Production Engineering, NISSAN MOTOR CO., LTD., 560-2, Okatsukoku, Atsugi-city, Kanagawa-pref. 243-0192, Japan.

 © 2012 American Institute of Physics

Reuse of AIP Publishing content is subject to the terms at: https://publishing.aip.org/authors/rights-and-permissions. Download to IP: 150.69.123.200 On: Wed, 26 Oct 2016 05:48:03

A semiconductor film was placed near the surface of piezoelectric crystal in the fringe field of a surface-acoustic Rayleigh wave. The traveling electric wave produces, in the semiconductor, a charge wave which in turn couples with the electric wave and produces a current. Since the current is proportional to the square of the field, there is a dc component which can be measured as an opencircuit acoustoelectric voltage by placing two electrodes on the film. The acoustoelectric voltage yields the drift mobility of the charge carriers in the semiconductor. We have also studied the temperature dependences of C_{60} and carbon nanotube films by using this method in our previous works.[18,19]

Based on the above results, we found in this study that the traveling-wave energy loss in a semiconductor is proportional to Joule heat caused by current of the charge wave. Therefore, we can determine concentration and mobility of the carriers in semiconductor by measuring the traveling-wave loss. A strong temperature dependence of carrier mobility due to higher measurement frequencies enables us to determine the bound states of the impurity atom by using Arrhenius plot. Four bound states have been observed in the accuracy close to far-infrared absorption measurement. Having found the expressions for both short-circuit current and open-circuit voltage due to the traveling-wave, we will show theoretically the loss due to the carriers excited from the bound states of impurity atom in semiconductor.

II. THEORY OF THE TRAVELING-WAVE METHOD

A theory for calculating potential distribution in the semiconductor due to the electric field created by surface acoustic wave on the surface of the piezoelectric crystal has been reported.[17,20] In this theory, a quasi-static approximation of the potential was used because propagation velocity of the SAW, v_s, is much less than the light velocity. Also, Laplace equation for the potential was assumed to hold in the media of both the semiconductor and the piezoelectric. For the semiconductor with dc conductivity σ_0, dielectric constant $\epsilon_r\epsilon_0$, and the thickness larger than the wavelength of the SAW, the potential ϕ in the semiconductor, the short-circuit dc current I_{ae}, and the open-circuit voltage V_{ae} are as follows:[17]

$$\phi = \phi_0\{A\cosh[k(y-h)] - B\sinh[k(y-h)]\} \times \exp[i(\omega t - kz)] \ , \tag{1}$$

$$I_{ae} = \sigma_0\left(\frac{\mu}{v_s}\right)Wk|A_\infty|^2\left(\frac{\phi_0^2}{2}\right), \tag{2}$$

$$V_{ae} = \left(\frac{\mu}{v_s}\right)Lk^2\left(\frac{1}{kd}\right)|A_\infty|^2\left(\frac{\phi_0^2}{2}\right), \tag{3}$$

where the SAW propagates along the z direction and the semiconductor and the piezoelectric arrange parallel along the y direction. Also, L, W, and d are length, width, and thickness of the semiconductor, respectively. μ is carrier mobility in the semiconductor and h is a distance between the semiconductor and the SAW device. k and ω are wavevector and angular frequency of the SAW. The ϕ_0 is given by the potential at the surface of the piezoelectric, and $|A_\infty|$ is the attenuation factor depending on dc conductivity, and dielectric constant of the semiconductor as well as frequency of the traveling SAW. In the conditions of this study, $|A_\infty|$ is close to unit.

We can obtain the Joule heat caused by the traveling-wave in the semiconductor as follow:

$$P = V_{ae}I_{ae}. \tag{4}$$

The Joule heat density in the semiconductor becomes

$$p = \frac{P}{LWd} = \sigma_0\mu^2\omega^2\frac{1}{d^2}\left(\frac{|A_\infty|}{v_s}\right)^4\frac{\phi_0^4}{4} = \gamma\sigma_0\mu^2\omega^2, \tag{5}$$

where γ is a constant independent to temperature. We see in Eq. (5) that the traveling-wave loss through the semiconductor is related to σ_0 and μ of the semiconductor as well as frequency of the traveling-wave.

We assume that the traveling-wave loss in the semiconductor, w, is proportional to the Joule heat p, and substitute σ_0 into Eq. (5). We have

$$w = \frac{V_{out}}{V_{in}} = \gamma qn\mu^3\omega^2 = \gamma q\mu^3\omega^2 N_c e^{-E_a/k_BT}, \tag{6}$$

where T is absolute temperature, N_c is effective density of states in the conduction band bottom, E_a is activation energy of the electrons excited from an impurity bound state to the conduction band, and n is the density of the free carriers. V_{in} and V_{out} are the input and output signal voltages to generate the traveling-wave. In the case of n–type Si, the mobility is dominated by both lattice and ion scatterings. It is a function of temperature and is proportional to $T^{-3/2}$ for lattice scattering and $T^{3/2}$ for ion scattering,[21] respectively. Therefore, we have result from Eqs. (5) and (6) as follows:

$$w = p \propto T^{-x(\omega)}\omega^2 e^{-E_a/k_BT}, \tag{7}$$

where $x(\omega) > 0$. With increasing temperature, the traveling-wave energy loss increases as e^{-E_a/k_BT} and decreases as $T^{-x(\omega)}$.

If we consider the bound state of 42.7 meV which is the ionization energy of the Sb atom in Si, the loss w calculated by Eq. (7) is shown in Fig. 1 as a function of inverse temperature. The loss at $x(\omega) = 0$, 5, and 10 for $\omega = 1$ is shown in Fig. 1(a). The loss decreases as a function of $T^{-x(\omega)}$ at high temperature side and increases as a function of e^{-E_a/k_BT} at low temperature side. In addition to the curve for $x(\omega) = 0$, the increase of the $x(\omega)$ value results in an asymmetrical peak which shifts toward lower temperatures. On the other hand, the increase in frequency ω leads to a symmetrical peak on the loss as shown in Fig. 1(b) where the vertical axis is shown in linear scale.

We have discussed the energy loss of the carriers excited from a bound state above. If the value of $x(\omega)$ is larger enough, more peaks relating to various bound states will be observed on temperature dependence of the traveling-wave loss.

In this study, the traveling-wave energy loss is obtained from signal attenuation, V_{out}/V_{in}. In order to analyze the

Reuse of AIP Publishing content is subject to the terms at: https://publishing.aip.org/authors/rights-and-permissions. Download to IP: 150.69.123.200 On: Wed, 26 Oct 2016 05:48:03

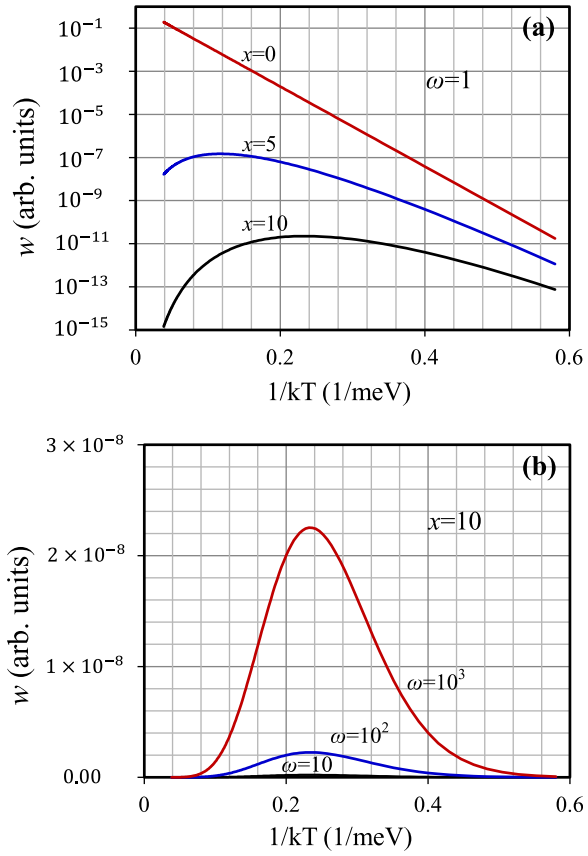

FIG. 1. Joule loss of the free electrons excited from the bound state $1s$ (A_1) of Sb atom in Si as a function of inverse temperature (a) for $\omega = 1$ and $x(\omega) = 0$, 5, and 10, (b) for $x(\omega) = 10$ and $\omega = 10$, 100, and 1000.

relationship between the loss and the bound state, the arrangement of the Si sample and the SAW device is shown in Fig. 2(a). The SAW device couples electrically with the electrons in the Si crystal sample through the traveling-wave. The traveling-wave loses its energy as the Joule heat by drifting the electrons in the Si crystal. Therefore, in general, the SAW device is as a source with an internal resistance Z_0' in order to supply electrical power to the measurement sample with a load resistance Z, as seen at the right-hand side of Fig. 2(a). When Z is much less than Z_0 as shown at the left-hand side of Fig. 2(b), the current density i_{ae} in the sample is constant. The Joule heat density becomes $p = i_{ae}^2/\sigma$, and thus the loss $w = p$ is proportional to reverse conductivity of the sample. This case corresponds to measurement of high conductivity samples such as superconductors, metals, and graphite. On the other hand, when Z is much larger than Z_0 as shown at the right-hand side of Fig. 2(b), strength of the electric field E_{ae} in the sample is constant, so that the Joule heat density becomes $p = E_{ae}^2\sigma$ and w is proportional to conductivity of the sample. This case corresponds to measurement of low conductivity samples such as light-doped semiconductors and insulators. The transition between two cases depends on the ratio of Z/Z_0. In the measurement of the Sb–doped Si crystal in this study, the loss w is proportional to the value of $E_{ae}^2\sigma$.

III. EXPERIMENTAL

The Sb-doped Czochralski Si wafer with donor concentration of $2 \times 10^{15}\,\mathrm{cm}^{-3}$ was used in this study. The Si crystal sample with dimensions of $10 \times 10 \times 0.5\,\mathrm{mm}^3$ was placed near the surface of the SAW device. The SAW device was fabricated on the surface of a 128° Y–X $LiNbO_3$ crystal. Its fundamental frequencies determined by the spacing of the interdigital transducer (IDT) were 50 and 200 MHz. Because the acoustic wavelengths are 80 μm for 50 MHz wave and 20 μm for 200 MHz wave, in order to obtain higher sensitivity and accuracies the gap between the Si sample and the SAW device was fixed using a polytetrafluoroethylene spacer with thickness of 5 μm. A dc pulse signal with amplitude of 30 V, width of 50 μs and frequency of 10 kHz was introduced to the input IDT electrode to generate the SAW.

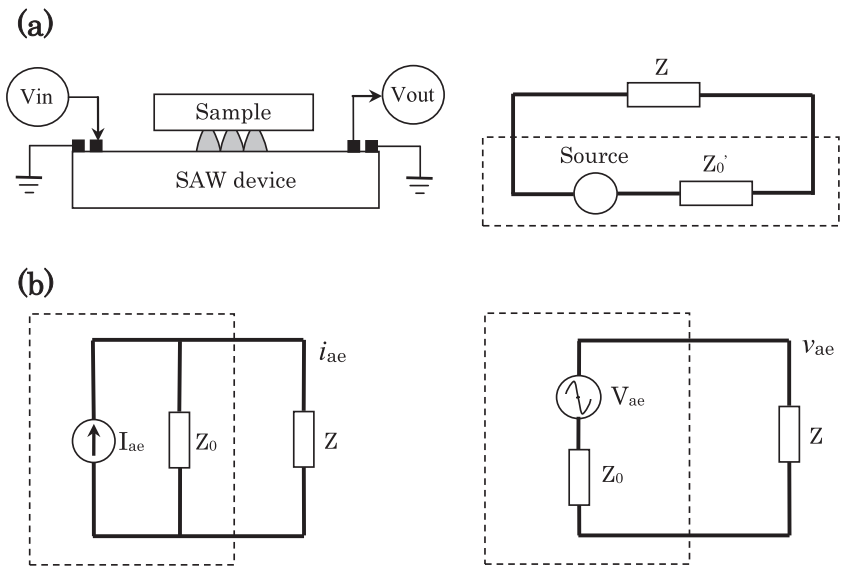

$Z \ll Z_0$, i_{ae} =constant,
$p = i_{ae}^2/\sigma$, $w \propto 1/\sigma$

$Z \gg Z_0$, v_{ae} =constant,
$p = E_{ae}^2\sigma$, $w \propto \sigma$

FIG. 2. (a) Arrangement of the Si crystal sample and the SAW device as well as their equivalent circuit. (b) Equivalent circuits of the measurement system for low- and high-resistance measurement samples.

Reuse of AIP Publishing content is subject to the terms at: https://publishing.aip.org/authors/rights-and-permissions. Download to IP: 150.69.123.200 On: Wed, 26 Oct 2016 05:48:03

After a delay of 4.5 μs, the SAW was detected by the output IDT electrode as an ac signal with frequency of 50 MHz or 200 MHz. In order to obtain the attenuation V_{out}/V_{in}, the input and output signals were processed using the Fourier-transform at real time. Typical input and output signals for the 50 MHz device are shown in Figs. 3(a) and 3(c), and the transformed signals are shown in Figs. 3(b) and 3(d), respectively. The attenuation $V_{out}/V_{in}$was obtained from the signal intensities after the Fourier-transform.

The Si crystal sample and SAW device were set in a cryostat chamber with a residual gas pressure of less than 2.0×10^{-5} Pa. The temperature of the Si crystal sample was controlled using both temperature controller (Model 331 S, LakeShore), and cryostat (D105, Iwatani Industrial Gases Corp.) in the range of $10 \sim 300$ K in steps of 1 K at the rate of 0.14 K min^{-1}. The input and output signals were observed using oscilloscope (WaveSurfer 452, LeCroy). Before the measurement, the Si crystal was treated at 450 K in the cryostat chamber in vacuum for a week to desorb the gases on its surface.

Because a quasistatic approximation of the traveling-wave potential was used, the effects of the magnetic field in the SAW can be ignored. The depth of the traveling-wave sank into the Si crystal is dominated by the electrostatic induction effect. We have estimated the depth, about 0.3 mm, less than the skin depth of an electromagnetic wave with the same frequency in the Si crystal, about 2 mm. We did not found any significant differences during the measurements of the Si crystal samples with various thicknesses above 0.5 mm.

Before the measurements of the traveling-wave loss, the temperature dependence of the loss in the piezoelectric crystal was also measured as a background. No significant variations were observed in the temperature range used in this study.

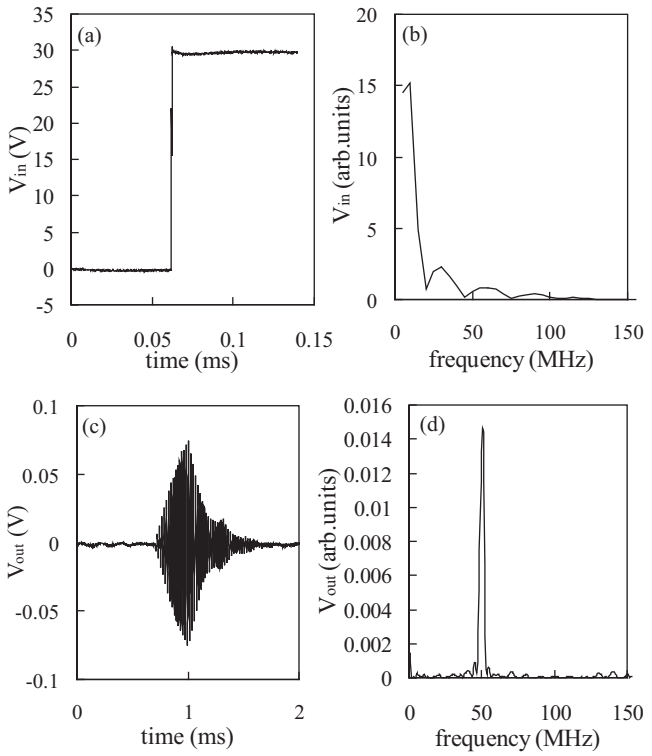

FIG. 3. Typical input (a) and output (c) signals, and Fourier-transformed input (b) and output (d) signals for the 50 MHz measurement.

IV. RESULTS

The traveling-wave loss in the Si crystal at the traveling-wave potential $\Phi_0 = 0.20$ V at the surface of the SAW device during the cooling process from 300 K to 20 K at frequency of 50 MHz is shown in Fig. 4 as a function of inverse absolute temperature. Three broad peaks with the shape similar to that in Fig. 1(a), which correspond to smaller x values, are observed. Also, a speedy increase, α, is seen at high temperature side. The three peaks distribute to a wide temperature range from 0.05 to 0.40 (1/meV) and on an increasing background with temperature. We will discuss later that the background is related to a dc conductivity of the Si sample and depends on the frequency of the traveling-wave. Using a calibration of the vertical axis, divided by T in order to remove the background, we obtained three activation energies of 42.7 meV, 32.7 meV, and 29.9 meV by Arrhenius plot. The activation energies are in good agreement with the bound states of Sb atom in Si crystal, $1s$ $A_1 = 42.7$ meV, $1s$ $T_2 = 32.9$ meV, and $1s$ $E = 30.6$ meV.[5]

As a comparison, the traveling-wave losses at 50 MHz during heating and cooling processes are shown in Fig. 5 as a function of inverse absolute temperature. No significant difference is observed during both heating and cooling processes.

We also measured the traveling-wave loss at frequency of 200 MHz. The losses at various potential of the traveling-wave at the surface of the SAW device, $\Phi_0 = 0.77$ V, 0.31 V, and 0.12 V, during cooling process are shown in Fig. 6 as a function of inverse temperature. The temperature dependence of the traveling-wave loss at 200 MHz is much different to that at 50 MHz. Several peaks are observed in a narrow temperature range from 0.1 to 0.25 (1/meV). Each peaks become more symmetrical and sharp, and the speedy

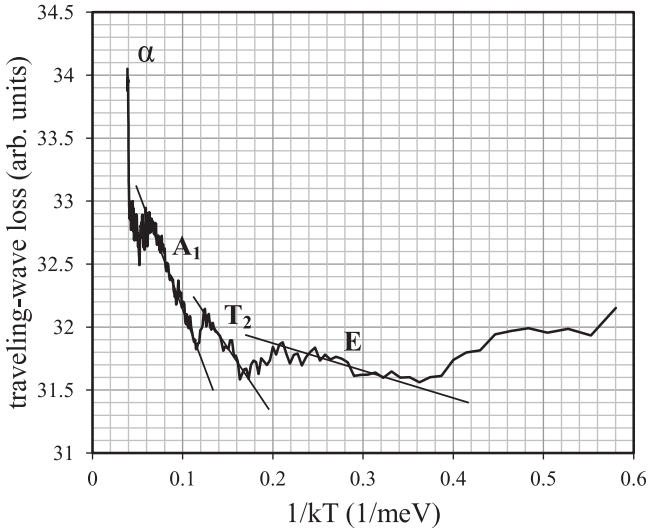

FIG. 4. Traveling-wave loss in the Si crystal at the traveling-wave potential $\Phi_0 = 0.20$ V at the surface of the SAW device during the cooling process from 300 K to 20 K at frequency of 50 MHz as a function of inverse absolute temperature.

Reuse of AIP Publishing content is subject to the terms at: https://publishing.aip.org/authors/rights-and-permissions. Download to IP: 150.69.123.200 On: Wed, 26 Oct 2016 05:48:03

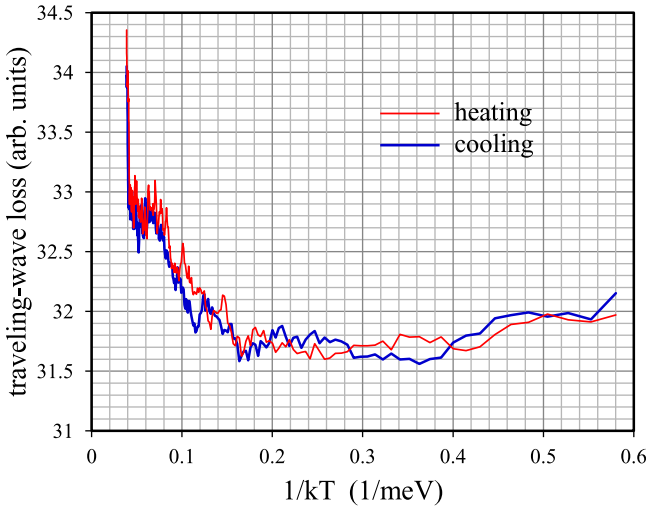

FIG. 5. Comparison of the traveling-wave energy losses at frequency of 50 MHz during heating and cooling processes as a function of inverse absolute temperature.

increase at high temperature side is observed as a peak, α, centered at 0.1 (1/meV). The number of the peaks which can be observed decreases with decreasing surface potential Φ_0. In addition to the peak α, other four peaks have high symmetry similar to that shown in Fig. 1(b). After the traveling-wave loss is divided by $T^{3/2}$, the activation energy corresponding to the four peaks is 42.5 meV, 32.5 meV, 29.5 meV, and 12.3 meV, respectively. They are in good agreement with the bound states of Sb atom in Si crystal, $1s$ $A_1 = 42.7$ meV, $1s$ $T_2 = 32.9$ meV, $1s$ $E = 30.6$ meV, and $2p^0 = 11.5$ meV.[5]

The activation energies obtained at the 200 MHz measurement are shown in Fig. 7 as a function of the surface potential Φ_0 of the traveling-wave. They increase with increasing surface potential and become saturate when the potential Φ_0 is large enough. The potential Φ_0 does not affect the saturation value of the each activation energies, but changes the number of the peaks which can be observed on the temperature dependence.

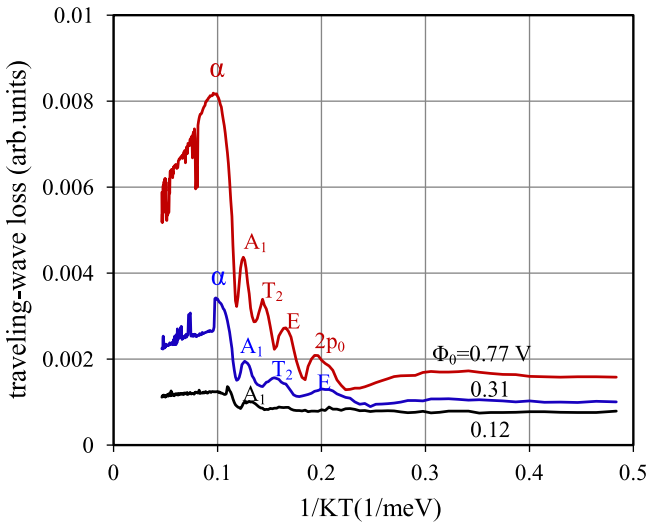

FIG. 6. Losses at various potential Φ_0 of the traveling-wave at the surface of the SAW device, $\Phi_0 = 0.77$ V, 0.31 V, and 0.12 V, during cooling process as a function of inverse absolute temperature.

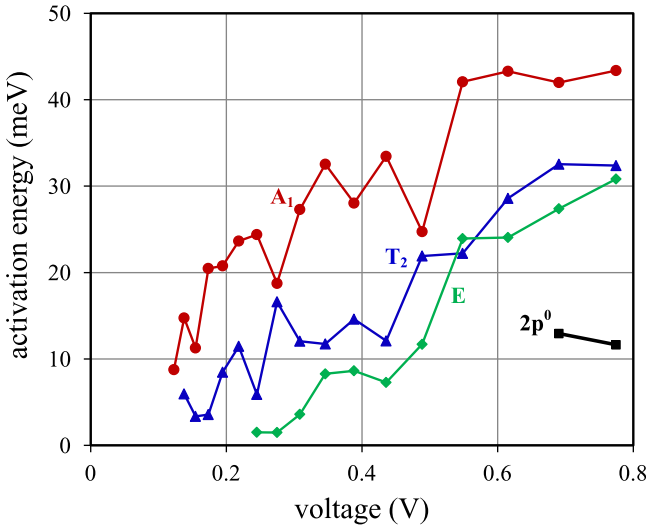

FIG. 7. Activation energies obtained at the 200 MHz measurements as a function of the surface potential Φ_0 of the traveling-wave.

The temperature dependences of the traveling-wave loss at frequency of 200 MHz during heating and cooling processes are shown in Fig. 8. The inset in the figure shows the details of the loss during heating process. The number of the peaks is the same to that during cooling process, but the peaks shift to higher temperatures. The results indicate that the electrons bound around Sb atoms are excited to the conduction band at higher temperatures during the heating process. Namely, the bound states of the Sb atom increase during heating process than that during cooling process. This is related to a decrease in dielectric constant of the Si crystal.

The activation energies corresponding to the loss peaks during the heating process are shown in Fig. 9 as a function of the surface potential Φ_0 of the traveling-wave. They increase with increasing potential Φ_0, but do not become saturate at higher surface potentials. Also, the activation energies increase at various rates with increasing surface potential.

As a characteristic parameter reflecting the shift of the loss curves during heating and cooling processes, the

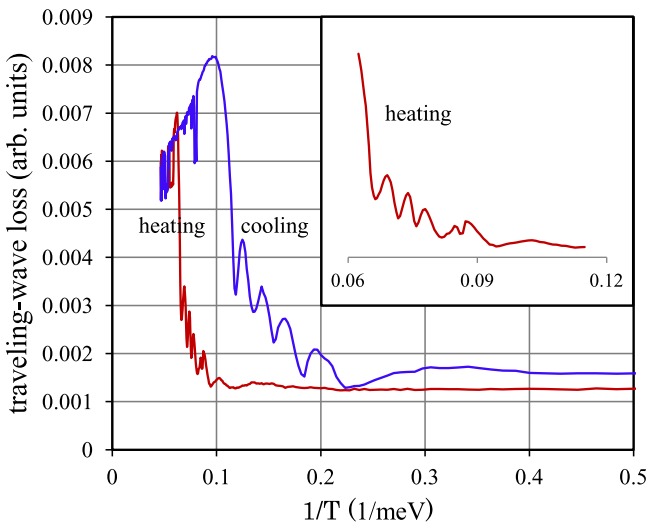

FIG. 8. Temperature dependences of the traveling-wave loss at frequency of 200 MHz during heating and cooling processes. The inset shows the details during heating process.

Reuse of AIP Publishing content is subject to the terms at: https://publishing.aip.org/authors/rights-and-permissions. Download to IP: 150.69.123.200 On: Wed, 26 Oct 2016 05:48:03

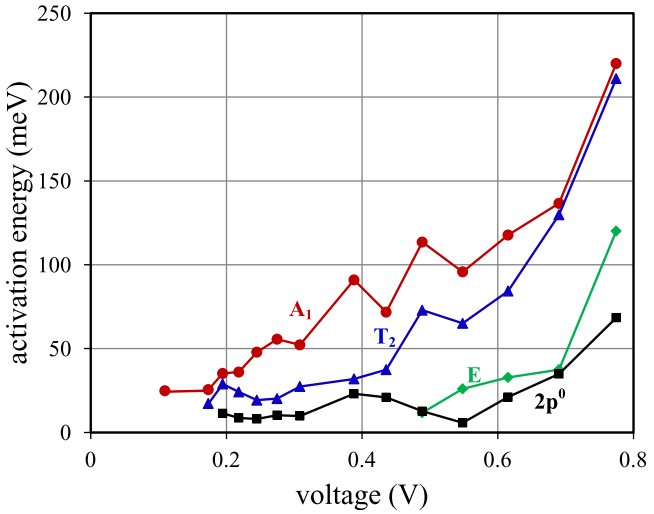

FIG. 9. Activation energies corresponding to the loss peaks during heating process as a function of the surface potential Φ_0 of the traveling-wave.

temperature difference between the α peaks, ΔT, is shown in Fig. 10 as a function of the surface potential Φ_0. The difference ΔT is constant, about 60 K, until the potential reaches 0.6 V, but increases at larger potentials. This may be corresponded to the results in Fig. 7 that the activation energies become saturate when Φ_0 is larger than 0.6 V. The potential dependence of the difference ΔT indicates that high electric field strength affects the screening effects of the bound and free electrons in the Si crystal. In fact, the maximum of the electric field strength in the Si crystal for $\Phi_0 = 0.77$ V is 96 V/cm for the 50 MHz device and 380 V/cm for the 200 MHz device, respectively. These values are much lower than the electric field in which electron velocity becomes saturate.

V. DISCUSSION

We are now in a position to discuss the mechanisms of the bound state measurement by the traveling-wave method on the base of the above results. We will discuss the effects from the traveling-wave and the Si crystal.

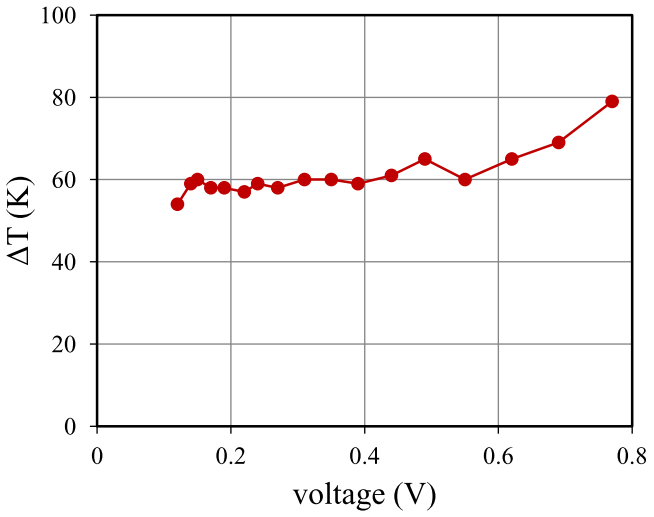

FIG. 10. Temperature difference ΔT between the α peaks on the loss curves at frequency of 200 MHz during heating and cooling processes as a function of the surface potential Φ_0.

A. Loss of the traveling-wave in Si crystal

For a *n*–type Si crystal, its conductivity changes with temperature. With decreasing temperature, an exponential decrease of the conductivity is observed in the intrinsic region. When the conductivity enters the extrinsic region where the electron concentration is constant, the conductivity rises because the mobility of the electron increases, for the simplest case $\mu \propto T^{-3/2}$. At still lower temperatures, the impurity region, there is the carrier freeze-out resulting in decrease of the conductivity. Therefore, there is a peak of the conductivity around the boundary between the extrinsic and impurity regions.[22] This peak corresponds to an energy level in the forbidden band, the impurity bound level. The impurity bound level in Si can be obtained by analyzing temperature-dependent concentration of free carriers in the freeze-out process. In this study, the traveling-wave loss depends strongly on temperature as described in Eqs. (5)–(7). The Joule loss of the carriers excited from an impurity level forms a peak on which the loss increases by e^{-E_a/k_BT} and decreases by $T^{-x(\omega)}$ with increasing temperature. If the peak is strong enough in intensity and small enough in width, we will observe the loss due to the carriers from more levels of impurity atoms. As described above, higher frequencies can shape and increase the loss peaks as shown in Fig. 1(b). Therefore, this measurement method enables us to observe a small change of the traveling-wave loss on its temperature dependence, and thus to determine the bound states of Sb atom in Si in high accuracy.

B. Effects of the traveling-wave frequency

Higher frequencies of the traveling-wave result in larger losses of the wave in Si crystal. As shown in Eqs. (5)–(7), the loss increases with the square of the frequency. This effect leads to shaper loss peaks on its temperature dependence as shown in Figs. 4–6.

Also, the Joule heat increases with increasing frequency as described in Eqs. (5)–(7). For a dc signal, the Joule loss *p* is proportional to σ_0 or $nT^{-3/2}$. But, for a high frequency signal, the Joule loss is proportional to $\sigma_0\mu^2\omega^2$ or $nT^{-9/2}$. As a result, we can observe more peaks on temperature dependence of the traveling-wave loss at higher frequencies because the $1/k_BT$ axis is compressed by the factor of $T^{-9/2}$, namely, the $1/k_BT$ axis becomes $(1/k_BT)^3$.

The frequency also affects polarization properties of the Sb atoms and electrons in the Si. In particular, the frequencies of 50 MHz and 200 MHz used in this study are in the boundary between dopant-controlling and electron-controlling polarizations.

C. Effects of lattice vibration

The dielectric constants of *n*–type, *p*–type, and compensated Si crystals have been studied in wide temperature and frequency regions. At frequencies above 10 MHz, the electronic polarizability of Si only is observed. At frequencies below 10 MHz, the atomic polarizablity of dopants is predominant.[23] For frequencies used in this study, 50 MHz and 200 MHz, there are different temperature dependences of the

Reuse of AIP Publishing content is subject to the terms at: https://publishing.aip.org/authors/rights-and-permissions. Download to IP: 150.69.123.200 On: Wed, 26 Oct 2016 05:48:03

dielectric constant of the Si crystal due to both effects of the electronic and atomic polarizalities. The dielectric constant at 50 MHz is almost constant at temperatures below 200 K. On the other hand, the dielectric constant at 200 MHz decreases with increasing temperature from 4.2 K to 200 K.[23] The electronic polarization becomes more important in the case of 200 MHz. Based on the Bohr theory, the bound states of the Sb atom in Si can be written as $E_n = -q^4 m_e^*/8\epsilon_r^2\epsilon_0^2 h^2 m^2$ where m_e^* is effective mass of electron, and m is integral number. The value E_n of the bound states is sensitive to the dielectric constant $\epsilon_r\epsilon_0$. Therefore, there are various temperature dependences of the traveling-wave loss for different frequencies. In the case of 50 MHz, the dielectric constant does not change at temperatures below 200 K, so that there are the same temperature dependences during heating and cooling processes as shown in Fig. 5. On the other hand, in the case of 200 MHz, the values of the activation energies obtained at higher temperatures during heating process are larger than that at lower temperatures during cooling process as shown in Figs. 6–9. This is due to the difference from the dielectric constant. Therefore, we can conclude that lattice vibration decreases the electronic polarization of the Si crystal at 200 MHz.

D. Effects of electronic polarization

As shown in Fig. 8, the electrons in the bound states in the forbidden band are completely excited at temperatures above 193 K (0.06/meV) during the heating process and are frozen out from the conduction band at temperatures below 25 K (0.45/meV) during the cooling process. Unlike the case of 50 MHz in which the dielectric constant $\epsilon_r\epsilon_0$ is independent of temperature, it decreases with increasing temperature from 25 K to 200 K in the case of 200 MHz due to the electronic polarization. Two factors influence the dielectric constant of the Si crystal. One is the effects from the lattice vibration. A strong lattice vibration will decrease the electronic polarization in the Si crystal. Another one is the effects of the free electrons. The concentration of the free electron is exponential to the temperature. The difference of the concentration at high- and low-temperature sides results in a hysterical properties on the traveling-wave loss during the heating and cooling processes. During the heating process starting from low-temperature side, the electrons in the ground states cannot be excited until temperature reaches to about 116 K (0.10/meV) due to a large spacing of 19.1 meV as shown in Fig. 8. This low electron concentration leads to smaller dielectric constants, and thus larger bound states appeared at high-temperature side. On the other hand, the electrons have been completely excited to the conduction band when start the cooling process at 300 K. This nonlinear variation of the concentration of the free electrons with temperature is responsible for the hysterical properties on the traveling-wave loss.

E. Effect of the electric field strength

The electric field with high strength can effectively drift the free carriers in the Si crystal and thus increase the screening effects on potential of the impurity atoms. The effects are particularly reflected to the bound states of the Sb atom as well as the temperature dependence of the traveling-wave loss. As shown in Fig. 10, the effects of the electric field strength are observed for the surface potentials greater than 0.6 V. In fact, strength of the surface potential depends on both the IDT electrode structure and the amplitude of the input high frequency signal. The effect of the electric field strength can be ignored in the 50 MHz measurement in which highest Φ_0 is 96 V/cm. But, it can be observed in the 200 MHz measurement in which highest Φ_0 is 380 V/cm. High electric field results in a large ΔT, namely, a large difference on the concentrations of the free carriers at high- and low-temperature sides.

F. Effects of the dc conductivity

The α peak on the temperature dependence of the traveling-wave loss is observed above 290 K (0.04/meV) for 50 MHz as well as at 116 K (0.10/meV) during cooling process and at 193 K (0.06/meV) during heating process for 200 MHz, respectively. The α peak and the background under the loss peaks are corresponding to the temperature dependence of the dc carrier mobility of the Si crystal. Previous experiments have observed a peak of carrier mobility on its temperature dependence for *n*–type Si crystal.[21] Position of the peak depends on the donor concentration and the applied electric field. The decreases around the peak are due to lattice scattering at high temperature side and impurity ion scattering at low temperature side. The peak shifts with the donor concentration and appears at 320 K for $10^{19}\,cm^{-3}$, at 270 K for $10^{18}\,cm^{-3}$ and below 100 K for $10^{16}\,cm^{-3}$ of the concentration.[21] In the high-frequency measurement of this study, the traveling-wave changes effectively the balance between lattice and ion scatterings as well as their temperature dependences. As shown in Fig. 8, the α peak during heating process appears at 193 K due to low concentration of the carriers. But, there is the same temperature dependence at temperatures above 193 K during the heating and cooling processes.

VI. CONCLUSION

We have studied the traveling-wave energy loss in the Sb-doped Si crystal by pleasing the crystal near the surface of SAW device. The temperature dependences of the loss are measured at various frequencies of the traveling-wave. The bound states of the Sb atom, 1*s* (A_1), 1*s* (T_2), 1*s* (E), and $2p^0$ can be determined by the Arrhenius plot of the temperature-dependent loss of the traveling-wave in high accuracy. We also found that the loss is influenced by several parameters of the wave and the Si crystal such as the frequency and the strength of the traveling-wave as well as the dielectric constant of the Si crystal. The traveling-wave at higher frequencies such as 50 and 200 MHz results in large collision probabilities of the free electrons with the Si lattice and leads to a larger Joule loss and a strong temperature dependence. The strong temperature dependence has made possible measurement of the bound states of the Sb atom in Si crystal by Arrhenius plot. The dielectric properties of the Si crystal, which depend on the traveling-wave frequency and the

Reuse of AIP Publishing content is subject to the terms at: https://publishing.aip.org/authors/rights-and-permissions. Download to IP: 150.69.123.200 On: Wed, 26 Oct 2016 05:48:03

electronic polarization of the Si crystal, play an important role in the measurement of the ground and excited states of the Sb atom in Si crystal. We have also measured the bound states of P, As, B, and In atoms in Si crystal by using this method as a comparison. Similar results will be reported elsewhere.

ACKNOWLEDGMENTS

This work was partially supported by Project No. 15–B01, Program of Research for the Promotion of Technological Seeds, Japan Science and Technology Agency (JST) as well as Grant-in-Aid for challenging Exploratory Research, No. 23651115, Japan Society for the Promotion of Science (JSPS).

[1]S. G. Pavlov, R. Kh. Zhukavin, E. E. Orlova, V. N. Shastin, A. V. Kirsanov, H. W. Hubers, K. Auen, and H. Riemann, Phys. Rev. Lett. **84**, 5220 (2000).
[2]S. G. Pavlov, R. Eichholz, N. V. Abrosimov, B. Redlich, and H. W. Hubers, Appl. Phys. Lett. **98**, 061102 (2001).
[3]B. E. Kane, Nature (London) **393**, 133 (1998).
[4]J. L. O'Brien, S. R. Schofield, M. Y. Simmons, R. G. Clark, A. S. Dzurak, N. J. Curson, B. E. Kane, N. S. McAlpine, M. E. Hawley, and G. W. Brown, Phys. Rev. B **64**, 161401 (2001).
[5]F. Bassani, G. Iadonisi, and B. Preziosi, Rep. Prog. Phys. **37**, 1099 (1974).
[6]J. H. Reuszer and P. Fisher, Phys. Rev. **135**, A1125 (1964).
[7]R. L. Aggarwal and A. K. Ramdas, Phys. Rev. **140**, A1246 (1965).
[8]S. Aymeloglu and J. N. Zemel, IEEE Trans. Electron Devices **23**, 466 (1976).
[9]D. V. Singh, K. Rim, T. O. Mitchell, J. L. Hoyt, and J. F. Gibbons, J. Appl. Phys. **85**, 985 (1999).
[10]H. Yuan, H. Zhang, and F. Lu, Semicond. Sci. Technol. **24**, 085004 (2009).
[11]P. P. Debye and E. M. Conwell, Phys. Rev. **93**, 693 (1954).
[12]J. H. Collins, K. M. Lakin, C. F. Quate, and H. J. Shaw, Appl. Phys. Lett. **13**, 314 (1968).
[13]H. Hanebrekke and K. A. Ingebrigtsen, Electron. Lett. **6**, 520 (1970).
[14]K. A. Ingebrigtsen, J. Appl. Phys. **41**, 454 (1970).
[15]L. A. Coldren and G. S. Kino, Appl. Phys. Lett. **18**, 317 (1971).
[16]T. Shiosaki, T. Kuroda, and A. Kawabata, Appl. Phys. Lett. **26**, 360 (1975).
[17]H. Fritzsche, Phys. Rev. B **29**, 6672 (1984).
[18]Y. Sun, Y. Yamasaki, K. Kirimoto, T. Miyasato, J. K. Wigmore, H. Moriyama, and T. Takase, Appl. Phys. Lett. **82**, 34 (2003).
[19]Y. Sun, T. Miyasato, K. Kirimoto, and M. Kusunoki, Appl. Phys. Lett. **86**, 223108 (2005).
[20]H. Fritzsche and K. J. Chen, Phys. Rev. B **28**, 4900 (1983).
[21]S. M. Sze, *Semiconductor Devices* (Wiley, New York, 1985), p. 33.
[22]B. I. Shklovskii and A. L. Efros, *Electronic Properties of Doped Semiconductors* (Springer-Verlag, Berlin, 1984), p. 75.
[23]A. Smakula, N. Skribanowitz, and A. Szorc, J. Appl. Phys. **43**, 508 (1972).

Reuse of AIP Publishing content is subject to the terms at: https://publishing.aip.org/authors/rights-and-permissions. Download to IP: 150.69.123.200 On: Wed, 26 Oct 2016 05:48:03